Terahertz lasers based on optically pumped multiple graphene structures with slot-line and dielectric waveguides

V. Ryzhii,[1,2,a)] A. A. Dubinov,[1,3] T. Otsuji,[2,4] V. Mitin,[5] and M. S. Shur[6]
[1]*Computational Nanoelectronics Laboratory, University of Aizu, Aizu-Wakamatsu 965-8580, Japan*
[2]*Japan Science and Technology Agency, CREST, Tokyo 107-0075, Japan*
[3]*Institute for Physics of Microstructures, Russian Academy of Sciences, Nizhny Novgorod 603950, Russia*
[4]*Research Institute for Electrical Communication, Tohoku University, Sendai 980-8577, Japan*
[5]*Department of Electrical Engineering, University at Buffalo, State University of New York, New York 14260, USA*
[6]*Department of Electrical, Electronics, and Systems Engineering, Rensselaer Polytechnic Institute, Troy, New York 12180, USA*

(Received 14 November 2009; accepted 21 January 2010; published online 3 March 2010)

Terahertz (THz) lasers on optically pumped multiple-graphene-layer (MGL) structures as their active region are proposed and evaluated. The developed device model accounts for the interband and intraband transitions in the degenerate electron-hole plasma generated by optical radiation in the MGL structure and the losses in the slot or dielectric waveguide. The THz laser gain and the conditions of THz lasing are found. It is shown that the lasers under consideration can operate at frequencies $\gtrsim 1$ THz at room temperatures. © *2010 American Institute of Physics*. [doi:10.1063/1.3327212]

I. INTRODUCTION

Graphene, graphene nanoribbons, and graphene bilayers (see, for instance, Ref. 1) can be used in different terahertz (THz) devices.[2–9] Optical excitation of graphene can result in the interband population inversion and negative real part of the dynamic conductivity of a graphene layer σ_ω in the THz range of frequencies.[7–9] The negativity of the real part of the dynamic conductivity implies that the interband emission of photons with the energy $\hbar\omega$, where $\hbar$ is the reduced Planck constant, prevail over the intraband (Drude) absorption. If the THz photon losses in the resonant cavity are sufficiently small, the THz lasing can be realized in graphene-based devices with optical pumping.[10,11] In Refs. 10 and 11, the optically pumped THz lasers with a Fabry–Pérot resonator were considered. In this paper, we propose and evaluate the THz lasers based on multiple-graphene-layer (MGL) structures with a metal slot-line waveguide (SLW) or a dielectric waveguide (DW) pumped by optical radiation. The specific features of characteristics of the MGL-based lasers under consideration are associated with the frequency dependences of the absorption in the waveguides and the gain-overlap factor, which is sensitive to the spatial distribution of the THz electric field. As shown in the following, the characteristics of the lasers with SLW and DW are fairly similar, so that we will mainly focus on the device with SLW. This is in part because the structures with SLW exhibit somewhat better confinement, and can be used not only for MGL-based lasers with optical pumping but also in MGL-based injection lasers with lateral *p-i-n* junctions (both electrically induced[12–14] and formed by pertinent doping of MGL structure).

II. DEVICE MODEL

We consider lasers (a) with a MGL structure on a SiC or Si substrate with the side highly conducting metal strips and a highly conducting back electrode at the substrate bottom and (b) with a MGL structure on the top of a SiC or Si slab serving as a DW. The cross-sections (corresponding to the $y-z$ plane) of the device structures under consideration are schematically shown in Fig. 1. The axis x corresponds to the direction of the electromagnetic wave propagation, whereas the y and z directions are in the MGL structure plane and perpendicular to it, respectively (see Fig. 1). The MGL plane corresponds to $z=0$. The finiteness of the MGL structure thickness can be disregarded. It is assumed that the MGL structure under consideration comprises K upper GLs and a highly conducting bottom GL on a SiC substrate or K GLs (without the bottom GL) on a Si substrate. Epitaxial MGL structures with up to $K=100$ GLs with very long momentum relaxation time of electrons and holes ($\tau \simeq 20$ ps) were recently fabricated using the thermal decomposition from 4*H*-SiC substrate.[15] MGL structures without the bottom GL can be fabricated using chemical/mechanical reactions and

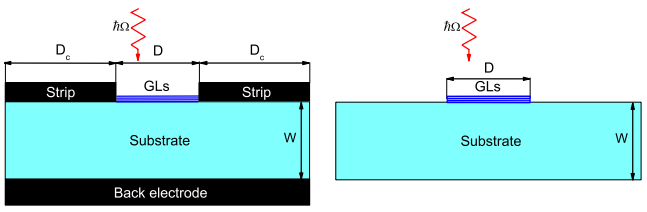

FIG. 1. (Color online) Schematic views of the device structures under consideration: (a) with a SLW and (b) with a DW.

[a)]Electronic mail: v-ryzhii@u-aizu.ac.jp.

transferred substrate techniques, which include chemically etching the substrate and the highly conducting bottom GL (Ref. 16) (or mechanically peeling the upper GLs) and transferring the upper portion of the MGL structure on a Si or equivalent transparent substrate. Since the electron density and the Fermi energy ε_F^B in the bottom GL is rather large ($\varepsilon_F^B \simeq 400$ meV),[17] the Drude absorption in this GL can be significant although it can be overcome by a strong emission from the upper GLs if their number is sufficiently large. The MGL structures without the bottom GL can exhibit significant advantages (see Ref. 11 and below).

It is assumed that the MGL structure is illuminated from the top by light with the energy of photons $\hbar\Omega$. The optical waveguide input of the pumping radiation is also possible. When $\hbar\Omega$ is close to $N\hbar\omega_0/2$, where $\hbar\omega_0 \simeq 0.2$ eV is the optical phonon energy and N is an integer, the photogeneration of electrons and holes and their cooling, associated with the cascade emission of optical phonons, result in an essentially occupation (population inversion) of low energy states near the bottom of the conduction band and the top of the valence band. At elevated electron and hole densities (i.e., at sufficiently strong optical pumping), the electron and hole distributions in the range of energies $\varepsilon \ll \hbar\omega_0$ in the kth GL ($1 \leq k \leq K$) can be described by the Fermi functions with the quasi-Fermi energies $\varepsilon_F^{(k)}$.

The quasi-Fermi energies in the GLs with $k \geq 1$ are mainly determined by the electron (hole) density in this layer Σ_k, i.e., $\varepsilon_F^{(k)} \propto \sqrt{\Sigma^{(k)}}$ and, therefore, by the rate of photogeneration $G_\Omega^{(k)}$ by the optical radiation at the kth GL plane. Considering the attenuation of the optical pumping radiation due to its absorption in each GL, one can obtain

$$G_\Omega^{(k)} = \frac{I_\Omega}{\hbar\Omega}\beta[(1-\beta)^{K-k} + (1-\beta_B)^2(1-\beta)^{K+k-1}]. \tag{1}$$

Here, I_Ω is the intensity of incident pumping radiation, $\beta = \pi e^2/\hbar c \simeq 0.023$, where e is the electron charge, c is the speed of light in vacuum, and $\beta_B = (4\pi/c)\mathrm{Re}\,\sigma_\Omega^B$. The latter quantity accounts for the absorption of optical pumping radiation in the bottom layer. A relationship between $\varepsilon_F^{(k)}$ and $G_\Omega^{(k)}$ is determined by the recombination mechanisms.[11] As a result, $\varepsilon_F^{(k)}$ can be expressed via the quasi-Fermi energy in the topmost GL $\varepsilon_F^T = \varepsilon_F^{(K)}$, which, in turn, is a function of the intensity of incident pumping radiation I_Ω.

Since the thickness of the MGL structure is small in comparison with the wavelength of THz radiation, the generation and absorption are determined by the real part of the net dynamic conductivity, which is the sum of the real parts of the dynamic conductivity of the bottom GL $\mathrm{Re}\,\sigma_\omega^B$ and other GLs $\sigma_\omega^{(k)}$

$$\mathrm{Re}\,\sigma_\omega = \mathrm{Re}\,\sigma_\omega^B + \mathrm{Re}\sum_{k=1}^{K}\sigma_\omega^{(k)}. \tag{2}$$

Considering the expressions for $\mathrm{Re}\,\sigma_\omega^B$ and $\mathrm{Re}\,\sigma_\omega^{(k)}$ obtained previously,[11] one can arrive at the following:

$$\mathrm{Re}\,\sigma_\omega = \left(\frac{e^2}{4\hbar}\right)\left\{\frac{4k_BT\tau_B}{\pi\hbar(1+\omega^2\tau_B^2)}\ln\left[1+\exp\left(\frac{\varepsilon_F^B}{k_BT}\right)\right] + \frac{8k_BT\tau}{\pi\hbar(1+\omega^2\tau^2)}\sum_{k=1}^{K}\ln\left[1+\exp\left(\frac{\varepsilon_F^{(k)}}{k_BT}\right)\right] + \sum_{k=1}^{K}\tanh\left(\frac{\hbar\omega - 2\varepsilon_F^{(k)}}{4k_BT}\right)\right\}. \tag{3}$$

Here, τ_B and τ are the electron and hole momentum relaxation times in the bottom and other GLs, respectively, T is the electron and hole temperature, and k_B is the Boltzmann constant. The first two terms in the right-hand side of Eq. (3) are associated with the intraband (Drude) absorption of THz radiation in all GLs, whereas the third term corresponds to the interband transitions. In the case of lasers without the bottom GL, one can use Eq. (3) formally setting $\tau_B = \infty$.

The electromagnetic waves propagating along the SLW was considered using the following equation, which is a consequence of the Maxwell equations:

$$\frac{\partial^2 E_\omega(y,z)}{\partial y^2} + \frac{\partial^2 E_\omega(y,z)}{\partial z^2} + \left[\frac{\omega^2}{c^2}\eta(y,z) - q^2\right]E_\omega(y,z) = 0. \tag{4}$$

Here, $E_\omega(y,z)$ the amplitude of the yth component of the THz electric field $E(t,x,y,z,) = E_\omega(y,z)\exp[i(qx-\omega t)]$, $\eta(y,z)$ is the complex permittivity, q is the wave number of the propagating mode. The quantities $E_\omega(y,z)$, $dE_\omega(y,z)/dz$, and $\eta^{-1}(y,z)d[\eta(y,z)E_\omega(y,z)]/dy$ are continuous at the interfaces between the layers with different refractive indices. The boundary conditions for the guided mode correspond to

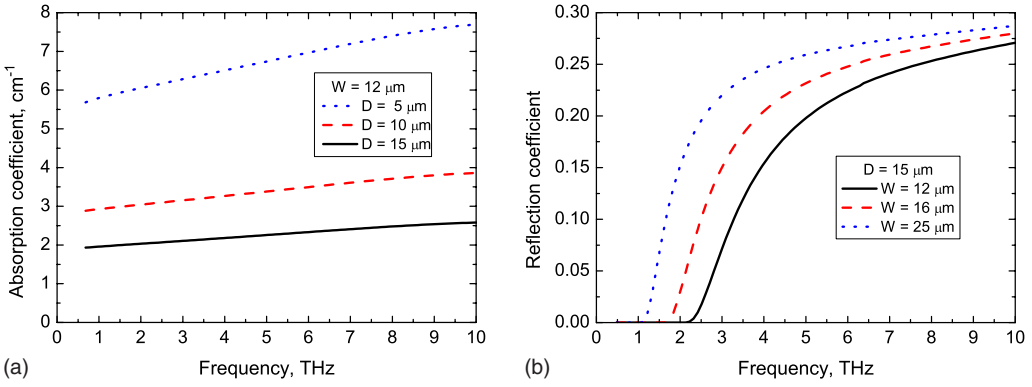

FIG. 2. (Color online) Coefficients of (a) absorption and (b) reflection vs frequency for SLWs with different geometrical parameters.

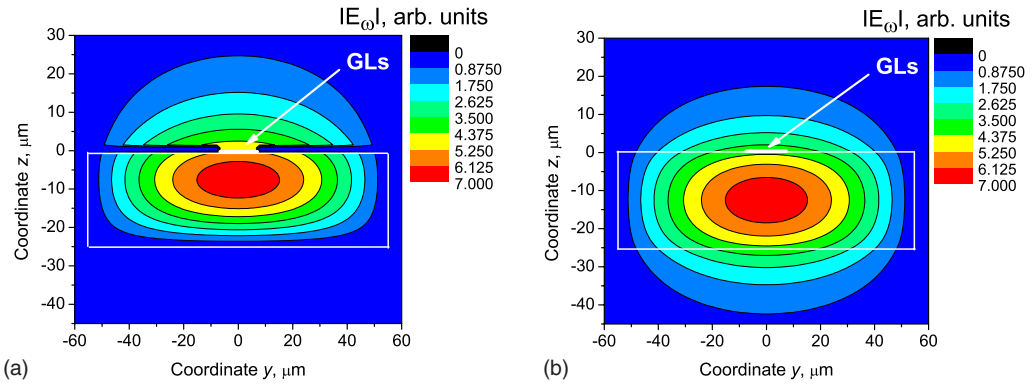

FIG. 3. (Color online) Spatial distributions of THz electric field (a) in SLW cross-section and (b) in DW cross-section.

the condition $E_\omega(y,z)\to 0$ at $y,z\to\pm\infty$. Equation (4) was solved numerically using the effective index and transfer-matrix methods (see, for instance, Refs. 18 and 19). The coefficient of absorption of the propagating mode α_ω and the coefficient of reflection from the interfaces between the laser structure edges and vacuum R were calculated using the following formulas, respectively: $\alpha_\omega=2\,\mathrm{Im}\,q$ and $R=|(q-q_0)/(q+q_0)|^2$, where $q_0=\omega/c$. The THz gain, which describes the attenuation or amplification of the propagating mode, under optical pumping can be calculated using the following formula:

$$g_\omega=\frac{4\pi\,\mathrm{Re}\,\sigma_\omega}{c\sqrt{\eta_S}}\Gamma_\omega-\alpha_\omega, \tag{5}$$

where

$$\Gamma_\omega=\frac{\int_{-D/2}^{D/2}|E_\omega(y,0)|^2dy}{\int_{-\infty}^{\infty}\int_{-\infty}^{\infty}|E_\omega(y,z)|^2dydz} \tag{6}$$

is the gain-overlap factor (in the case when σ_ω is independent of coordinate y) and η_S is the permittivity of the substrate (SiC or Si).

III. RESULTS AND DISCUSSION

Figure 2 shows the absorption coefficient α_ω of electromagnetic waves propagating along the SLW and the coefficient of reflection from the laser structure edges as function of frequency $\omega/2\pi$ calculated using Eq. (4) for different widths of the slot D and the strips D_c and the substrate thickness W. The strips and the back electrode are assumed to be made of Al. Examples of the spatial distributions of the THz electric field in the electromagnetic wave in laser structures with $D=15\ \mu$m at $\omega/2\pi=1.8$ THz in question are show in Fig. 3. The electric field distributions with the frequency dependences of the dynamic conductivity of the MGL structures obtained by solving Eq. (4) were substituted to Eqs. (5) and (6) to find the gain-overlap factor and the THz gain. Figures 4 and 5 show the frequency dependences of the THz gain g_ω calculated for the laser structures with (Fig. 4) and without (Fig. 5) bottom GL and with different structural parameters at different pumping conditions (different values of the quasi-Fermi energy) and at $T=300$ K. It was assumed that $\hbar\Omega=920$ meV, $\tau=10$ ps, and $\tau_B=1$ ps. The chosen value of τ is twice as small as that found experimentally[15] in MGL structures with different number of GLs (up to $K=100$). To take into account a shortening of the momentum relaxation time with significant increasing electron density,

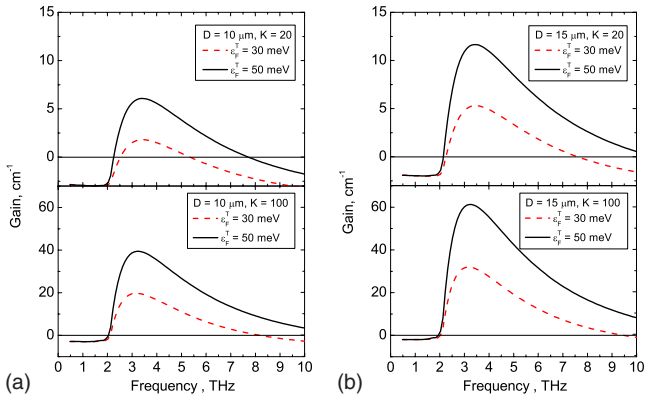

FIG. 4. (Color online) Frequency dependences of THz gain in laser structures with different width of the slot D and different number of GL K at different values of the quasi-Fermi energy ε_F^T: (a) $D=10\ \mu$m and (b) $D=15\ \mu$m.

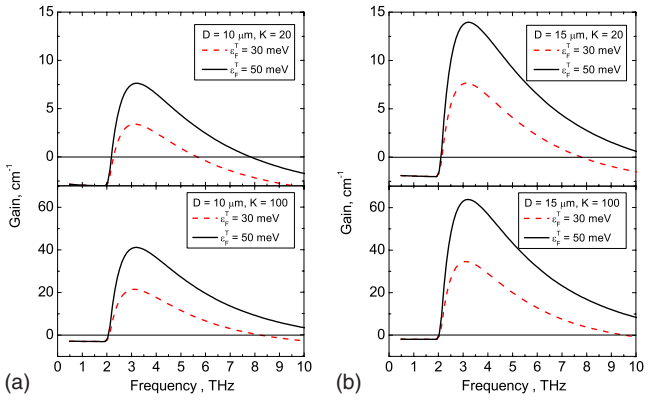

FIG. 5. (Color online) The same as in Fig. 4 but for laser structures without bottom GL.

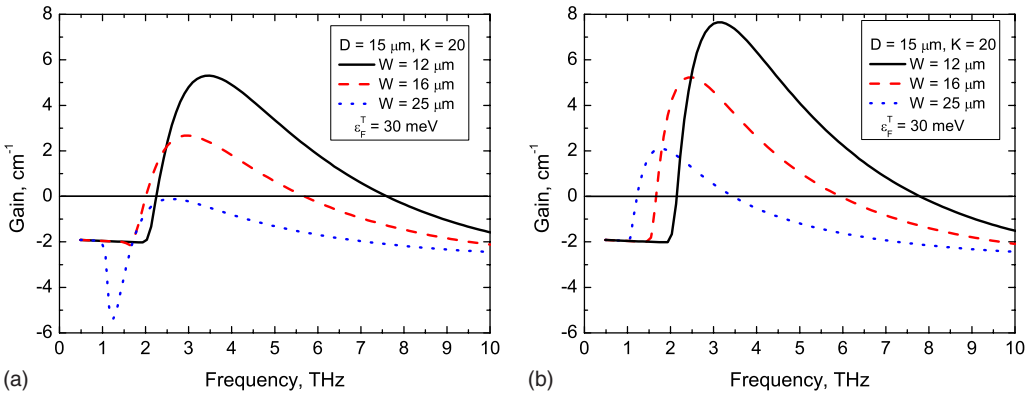

FIG. 6. (Color online) Comparison of THz gain vs frequency dependences in laser structures (a) with and (b) without bottom GL, and with different spacing between MGL structure and back electrode W.

this time in the bottom GL was chosen ten times shorter than in other GLs. As seen from comparison of the top panels of Figs. 4 and 5, the laser structures with and without the bottom GL (with $K=20$) exhibit qualitatively similar frequency dependences of the THz gain g_ω (at chosen geometrical parameters) but with somewhat higher maxima in the latter structures. In the case of the structures with $K=100$, these dependences (compare lower panels of Figs. 4 and 5) are virtually identical. The frequency $\omega_{\min}$ at which g_ω changes its sign is $\omega_{\min}/2\pi \simeq 2$ THz in the laser structures of both types. The latter is different from the situation in the MGL lasers with the Fabry–Pérot resonator,[11] in which eliminating the bottom GL can lead to a pronounced decrease in $\omega_{\min}$. This is attributed to the effect of SLW: the variation in the frequency results in a redistribution of the spatial distribution of the THz electric field and, hence, in a change in the gain-overlap factor. Due to this, the spacing between the MGL structure W and the back electrode affects the frequency dependences of the THz gain. Figure 6 shows these dependences calculated for different W. One can see that the height of the THz gain maxima decreases with increasing W. Simultaneously the frequency $\omega_{\min}$ shifts toward lower values. This shift is more pronounced in the laser structures without the bottom GL [compare Figs. 6(a) and 6(b)]. As seen from Fig. 6(b), $\omega_{\min}/2\pi$ can reach 1 THz. In the case of larger K and ε_F^T, as seen from Fig. 7, the THz gain in the range $\omega/2\pi \gtrsim 1-2$ THz can be rather large.

A decrease in the momentum relaxation time τ (which results in an enhancement in the Drude absorption) leads to an increase in $\omega_{\min}$ and to a decrease in $|\mathrm{Re}\ \sigma_\omega|$ in the range of frequencies, where $\mathrm{Re}\ \sigma_\omega < 0$. This is seen in Fig. 8.

The above results correspond to $T=300$ K. Lowering of the temperature should lead to widening of the frequency range where $\mathrm{Re}\ \sigma_\omega$ is negative and where g_ω can be positive. As a result, $\omega_{\min}$ might decrease with decreasing temperature. The latter is confirmed by the calculated temperature dependences of $\omega_{\min}$ shown in Fig. 9.

Figure 10 shows the frequency dependences of the THz gain calculated for laser structures with SLW and DW for $T=300$ K and $\tau=10$ ps. One can see that the maximum of the THz gain in the laser with SLW is somewhat higher than that in the laser with DW. This can primarily be explained by the effect of the spatial distribution of the THz electric field on the gain-overlap factor [compare Figs. 3(a) and 3(b)]. To maximize the THz gain at the desirable frequency, one needs carefully optimize the geometrical parameters.

Considering the propagation of the THz electromagnetic wave in the laser structure (with the length L in the

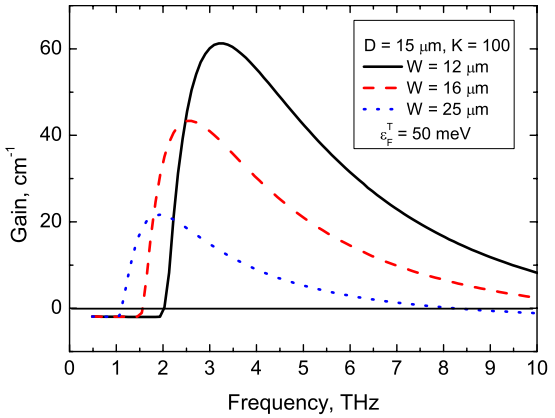

FIG. 7. (Color online) The same as in Fig. 6(a) but for $K=100$ and $\varepsilon_F^T = 50$ meV.

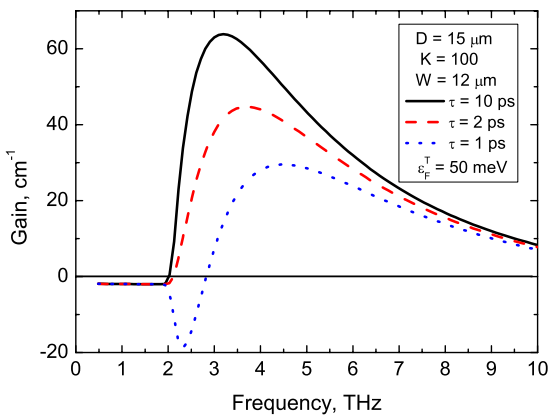

FIG. 8. (Color online) Frequency dependences of THz gain in laser structures (without the bottom GL) with different τ.

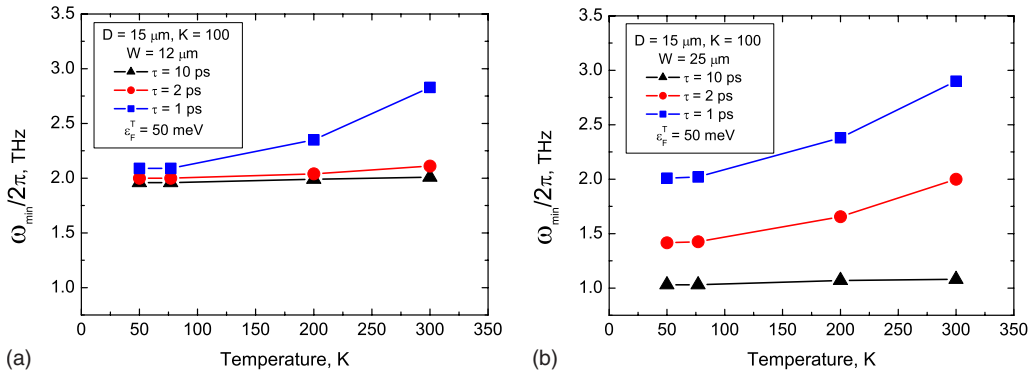

FIG. 9. (Color online) Temperature dependences of ω_{min} for laser structures with different τ: (a) $W=12$ μm and (b) $W=25$ μm.

x-direction) and its reflection from edges or from the external mirrors (with the reflective coefficients R_1 and R_2), the condition of lasing can be presented as

$$Lg_\omega > \ln\frac{1}{R_1R_2}. \tag{7}$$

For a laser structure with SLW with $D=15$ μm, $W=12$ μm, and $K=100$ at $\varepsilon_F^T=30-50$ meV and $\omega/2\pi=3.0$ THz, so that $R_1=R_2\simeq 0.05$ and $g_\omega\simeq 30-60$ cm^{-1} [see Figs. 2(b) and 4(b), respectively], one obtains $L>0.1-0.2$ cm. If $D=15$ μm, $W=25$ μm, and $K=100$ at $\varepsilon_F^T=50$ meV and $\omega/2\pi=1.5$ THz [$R_1=R_2\simeq 0.05$ and $g_\omega\simeq 10$ cm^{-1} as follows from Figs. 2(b) and 7, respectively], one obtains $L>0.6$ cm.

As shown above, at the quasi-Fermi in the topmost GL about $\varepsilon_F^T=30-50$ meV, the achievement of the THz lasing in the devices under consideration at room temperatures is feasible. At $T=300$ K the condition $\varepsilon_F^T\gtrsim 30$ meV corresponds to the electron and hole densities about 2×10^{11} cm^{-2}. Such densities can be obtained at reasonable optical powers (see Ref. 12 and the references therein).

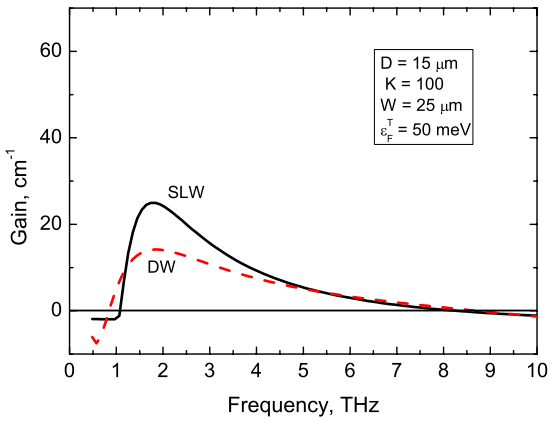

FIG. 10. (Color online) Comparison of the frequency dependences of THz gain in laser structures with SLW and DW,

IV. CONCLUSIONS

We proposed THz lasers with optical pumping based on MGL structures with waveguides and calculated their characteristics. The feasibility of lasing in the devices under consideration at the low end of the THz frequency range at room temperatures was demonstrated.

ACKNOWLEDGMENTS

The authors are grateful to V.V. Popov, M. Ryzhii, A. Satou, M. Suemitsu, and F.T. Vasko for fruitful discussions. This work was supported by the Japan Science and Technology Agency, CREST, Japan.

[1] A. H. Castro Neto, F. Guinea, N. M. R. Peres, K. S. Novoselov, and A. K. Geim, Rev. Mod. Phys. **81**, 109 (2009).
[2] F. T. Vasko and V. Ryzhii, Phys. Rev. B **77**, 195433 (2008).
[3] V. Ryzhii, V. Mitin, M. Ryzhii, N. Ryabova, and T. Otsuji, Appl. Phys. Express **1**, 063002 (2008).
[4] F. Xia, T. Mueller, R. Golizadeh-Mojarad, M. Freitag, Y. Lin, J. Tsang, V. Perebeinos, and P. Avouris, Nano Lett. **9**, 1039 (2009).
[5] V. Ryzhii and M. Ryzhii, Phys. Rev. B **79**, 245311 (2009).
[6] Y. Kawano and K. Ishibashi, Proceedings of the 34th International Conference on Infrared, and Terahertz Waves, Busan, Korea, 21–25 September 2009, (unpublished), W4A04.0380.
[7] V. Ryzhii, M. Ryzhii, and T. Otsuji, J. Appl. Phys. **101**, 083114 (2007).
[8] F. Rana, IEEE Trans. Nanotechnol. **7**, 91 (2008).
[9] A. Satou, F. T. Vasko, and V. Ryzhii, Phys. Rev. B **78**, 115431 (2008).
[10] A. A. Dubinov, V. Ya. Aleshkin, M. Ryzhii, T. Otsuji, and V. Ryzhii, Appl. Phys. Express **2**, 092301 (2009).
[11] V. Ryzhii, M. Ryzhii, A. Satou, T. Otsuji, A. A. Dubinov, and V. Ya. Aleshkin, J. Appl. Phys. **106**, 084507 (2009).
[12] V. V. Cheianov and V. I. Fal'ko, Phys. Rev. B **74**, 041403(R) (2007).
[13] M. Ryzhii and V. Ryzhii, Jpn. J. Appl. Phys., Part 2 **46**, L151 (2007).
[14] M. Ryzhii and V. Ryzhii, Physica E (Amsterdam) **40**, 317 (2007).
[15] P. Neugebauer, M. Orlita, C. Faugeras, A.-L. Barra, and M. Potemski, Phys. Rev. Lett. **103**, 136403 (2009).
[16] A. Bostwick, T. Ohta, T. Seyller, K. Horn, and E. Rotenberg, Nat. Phys. **3**, 36 (2007).
[17] F. Varchon, R. Feng, J. Hass, X. Li, B. Ngoc Nguyen, C. Naud, P. Mallet, J.-Y. Veuillen, C. Berger, E. H. Conrad, and L. Magaud, Phys. Rev. Lett. **99**, 126805 (2007).
[18] K. J. Ebeling, *Integrated Optoelectronics: Waveguide Optics, Photonics, Semiconductors* (Springer-Verlag, Berlin, 1993).
[19] M. Born and E. Wolf, *Principles of Optics: Electromagnetic Theory of Propagation, Interference and Diffraction of Light* (Pergamon, Oxford, 1964).